# Effect of Geometric Parameters on the Behavior of Bolted GFRP Pultruded Plates

Thérèse A. D. Tajeuna[1*], Frédéric Légeron[2], Sébastien Langlois[3], Pierre Labossière[4] and Marc Demers[5].

[1] Ph.D Student
Department of Civil Engineering
Université de Sherbrooke, Sherbrooke, Quebec, Canada, J1K 2R1
E-mail: **therese.tajeuna@USherbrooke.ca**

[2] Bridge and Tunnel UAE District Manager
Parsons Corporation
E-mail: **Frederic.legeron@parsons.com**

[3] Assistant Professor
Department of Civil Engineering
Université de Sherbrooke, Sherbrooke, Quebec, Canada J1K 2R1
E-mail: **Sebastien.Langlois@USherbrooke.ca**

[4] Professor
Department of Civil Engineering
Université de Sherbrooke, Sherbrooke, Quebec, Canada J1K 2R1
E-mail: **Pierre.labossière@USherbrooke.ca**

[5] Research Engineer
Department of Civil Engineering
Université de Sherbrooke, Sherbrooke, Quebec, Canada J1K 2R1
E-mail: **Marc.Demers@USherbrooke.ca**

[*]Author to whom all correspondence should be addressed

*Paper to be submitted to the Journal of Composites Materials (SAGE)*

**ABSTRACT**

This paper presents the effect of geometric parameters on the behavior of bolted GFRP pultruded plates for civil engineering applications. After a literature review, results of an experimental analysis investigating the behavior of GFRP-to-steel single-lap bolted connections are presented. Then, a finite element analysis validated by experimental data is used to evaluate the effects of the end-distance, side-distance, gage, pitch and plate properties on the strength and failure mode of the connection. A critical examination of geometric recommendations proposed in design references is presented. Bearing failure caused by contact of the bolt on the GFRP plate is usually defined as the preferred failure mode. With highly orthotropic plate, this type of failure was found to be less likely to occur when loading is applied in the pultruded direction. The investigation showed that the minimum end-distance and pitch-distance recommended by design references usually produce a connection with the maximum capacity. However, it was found that the minimum side-distance recommended by these references does not necessarily lead to the maximum capacity for one-bolt and for two-bolt in a column connections.

**Keywords**: Connection, bolt, pultruded GFRP, single-lap, FE analysis, failure mode, geometric parameters.

.

## Introduction

This study was initiated in the context of developing a high-strength and low-weight emergency repair solution for damaged railway structures. The use of Glass Fibre Reinforced Polymer (GFRP) pultruded plates was a promising option for this situation, their light weight making them easy to carry on site. Bolting GFRP plates to steel was viewed as a practical way of providing temporary repair work that could also be easy disassemble in the future. In addition, high strength, corrosion resistance, and low maintenance cost would be added benefits if the repair work had to stay in place for an extended period.

The main objective of this paper is to provide basic information on the static behavior of bolted joints between GFRP and steel in bridges and other civil engineering structures, to critically examine the geometric recommendations proposed in design references, and to identify optimum geometrical parameters to guarantee the high strength of such connections. In the first part of this paper, a literature review on the connection of GFRP plates is presented. In the second part of the paper, the data presented are complemented by an experimental study of GFRP-to-steel bolted connections performed by the authors. These results are compared to predictions according to a design reference. In the third part of the paper, a finite element (FE) analysis, validated by the experimental results, is used to study how the geometrical parameters of the connection are affecting its strength. In conclusion, optimum geometric parameters beyond which no further increase of the connection strength is observed are identified.

## Literature review

GFRP pultruded plates are made of E-glass fibres and resin. The pultruded plates are typically a combination of Continuous Strand Roving (CSR) and Continuous Strand Mat (CSM). The roving provides strength in the longitudinal (pultrusion) direction while the mat provides multi-

71 directional strength. CSM is considered to be isotropic since it contains chopped glass fibres that
72 are randomly oriented in the plane of the mat. The CSR is highly orthotropic and has higher
73 strength than CSM in the longitudinal direction. Therefore, the elastic properties of the plate
74 would depend on the proportion of these two constituents.
75 When connecting GFRP plates with bolts, the basic failure modes shown in Figure 1 can be
76 observed. They are similar to those observed for steel plate connections. Bearing of the bolt
77 produces either crushing in the loading direction (Figure 1a), tension failure through the net-
78 section (Figure 1b) or shear tear-out characterized by two parallel failure paths extending from
79 the bolt-hole to the plate end in the loading direction (Figures 1c and 1d). Another failure mode
80 for FRP pultruded plates is cleavage (Figure 1e), which is characterized by a single fracture line
81 extending from the bolt-hole to the end of the plate. Additional cracks in the net-section may also
82 appear. Failure by crushing is usually ductile and is therefore preferred to the other modes, which
83 are usually brittle.
84 The occurrence of the above failure modes depends on the geometrical parameters shown in
85 Figure 2. These include the number of shear planes ($x$), the end-distance ($e$), the side-distance ($s$),
86 the width ($w$), the pitch-distance ($p$) the gage-distance ($g$), the plate thickness ($t$), the bolt-hole
87 diameter ($d_h$), the bolt diameter ($d$), the number of bolts in the row ($n$), the number of bolts in the
88 column ($m$) and the total number of bolt in the connection ($N$). In a one-bolt or one-column bolts,
89 $s$ is equivalent to $0.5w$. Recommended values for these geometric parameters can be found in
90 design references such as: ASCE Pre-standard [1], EUROCOMP [2] and CNR-DT 205/2007 [3].
91 Manufacturers such as Strongwell [4], Fiberline Composites [5], and Creative Pultrusion [6] also
92 provide design manuals specific to the use of their products. Table 1 summarizes minimum
93 geometric recommendations for $e$, $s$, $p$ and $g$. These recommendations slightly differ from one
94 design reference to another. For example, FRP design standard [1] recommends a minimum

95 $p/d$=4 while EUROCOMP [2] design manual requires this ratio to be at least 3. ASCE Pre-
96 standard [1] recommends the maximum spacing of consecutive bolts in rows or columns ($p$ and
97 $g$) to be 12 times the minimum thickness of FRP material. However, it does not provide
98 recommendations for the edge distances ($e$ and $s$). Other references do not specify the maximum
99 values. Equations to calculate the connection strength corresponding to the failure modes
100 mentioned above can also be found in these design references.
101 Numerous studies of mechanically fastened joints in composite material have been reported in
102 the literature. Most have been conducted for the benefit of aeronautical and automotive industry.
103 An extensive review of several of these publications extending from 1978 to 2007 can be found
104 in Thoppul et *al*. [8]. For civil engineering application, Mottram and Turvey [9], present a review
105 of publication extending from 1980 to 2001 with regard to the appraisal of existing connections
106 design procedure for plate-to-plate bolted joints in pultruded FRP structural shapes and systems.
107 Girao and Mottram [10] recently reported similar work. In addition to the review of the plate-to-
108 plate bolted joint, [10] also addressed the design procedure of beam-to-column bolted joint.
109 However, this review does not include special topic of environmental effects. A reference and
110 bibliography database on research and development with pultruded FRP shapes and system can
111 be found in [11]. Most connections reported were tested with one bolt [12-33]. A few
112 experimental results with multi-bolt connections can also be found [34-40]. Specimens were
113 mostly loaded in double-lap configuration while few were loaded in single-lap configuration [19,
114 29, 30]. Figure 2(a) presents the geometric parameters as they are defined in this paper and the
115 typical case of single-lap and double-lap configurations. Single-lap connection differs from
116 double-lap configuration in that: double-lap configuration is to some extent symmetric with
117 respect to the center of the inner plate while single-lap configuration is non-symmetric. This non-
118 symmetry causes the inclination of the bolt in the bolt-hole during loading. Because of this

inclination, the bolt contact pressure in the bolt-hole becomes non-uniform through the plate thickness, leading to the out-of-plane deformation of the plate. The present study is limited to bolted connections of Glass Fibre Reinforced Polymer (GFRP) pultruded plates in the context of civil engineering applications. The following literature review focuses on to publications that bring an insight on the effect of geometric parameters as *e/d*, *s/d*, *g/d* or *p/d* on the connections strength of pultruded GFRP plates with tension loading parallel to the pultruded direction. The test results of Rosner and Rizkalla [13] on one-bolt connections suggest that connection strength and failure mode could be improved by increasing $w/d_h$ and $e/d_h$ ratios up to a limiting value of 5. At this ratio, bearing failure by crushing was the observed mode. Experimental results of Cooper and Turvey [15] reveal that the critical ratio at which bearing failure is observed depends on the clamping of the plates. These critical ratios were found to be $e/d$=5 and $w/d$=6 for lightly torqued and $e/d$=6.5 and $w/d$=10 for fully torqued connections. Experimental results of Ramaskrishna et *al*. [17] reveal that increasing *w/d* from 3 to 7 and keeping $e/d$=2 has no significant effect on the strength as shear associated to bearing controls the failure load. Study reported by Wang [23] on a 3.2 mm thick GFRP pultruded plate loaded in pin bearing condition reveal bearing failure for values of $w/d$=4 and $e/d$=1.5. The results also show no increase in the joint capacity for values of $e/d$>3. From his experimental results performed in single-lap one-bolt joint, Turvey [29] observed a threshold value of $e/d$=3 above which the average ultimate load and strength remain constant for any value of *w/d*. Below this threshold value, the average ultimate load increases with *e/d* and *w/d*. The author state that because of the effect of bending within the joint, failure modes of the single-lap joints tend to be more complicated than symmetric double-lap joints. Based upon the analysis and observation performed in the experimental investigation, Lee et *al* [33] recommend to maintain if possible $w/d$=5 and $e/d\geq$3. For multi-bolted connections, Hassan et *al*. [37] found that the ultimate capacity and the bearing

strength increased with the ratios of the side-distance-to-pitch (*s*/*p),* up to a limiting value of 1.2. Beyond this, no significant increase in the load-carrying capacity was measured. From their finite element analysis performed on multi-column of bolts, Girão Coelho et *al*. [40] recommend the minimum ratio of *g/d*=3 and *s/d*=2.5. In addition to these geometrical parameters, reported studies also provide information on either the influence of pultruded material orientation [13, 19-20,-23, 37], the type of fastener [14], washer size [12], hole clearance[16, 27], number of bolts and their arrangement [34, 37], environmental effect [18,21,22,24,25,26,31,39], and degree of orthotropy [12, 34]. Abd-El-Naby and Hollaway [12, 34] show that the failure mode is related to the proportion of CSM and CSR in the plate. Their experimental analysis shows that in plates with higher proportion of CSR than CSM, bearing failure is less likely to occur regardless of the connection length and width.

Although other experimental results in multi-bolt connections have been reported, the effect of pitch-distance has not been studied in details. In addition, only few data with single-lap bolted connections have been published. The experimental study on GFRP bolted plates reported in the next section was performed to cover these gaps in data. The investigation was performed on single-lap bolted connections. The results are compared to design strengths calculated using equations available in the ASCE Pre-standard [1]. Then, a FE analysis validated with experimental results is used to investigate the effect of *e*, *s*, *p* and the material properties. The results are used to critically examine the recommendations of design references.

## Experimental investigation of single-lap bolted connections

### *Overview of the experimental program*

Connections of GFRP to steel plates with one bolt or two bolts, in single-lap configuration, were tested. GFRP specimens were cut from 6.35 mm thick pultruded plates while steel specimens

were taken from 6.35 mm thick flat bars. All GFRP pultruded plates were loaded in the longitudinal direction to achieve maximum tensile strength. Connections with one bolt or with two bolts in a column were considered. ASTM A325 bolts with a 12.7 mm diameter and nominal washer were used. Bolts were tightened at finger tight plus one-half-turn of the nut. Two configurations were tested for one bolt connections. The single-lap configuration S20E30 had $s/d$=2 and $e/d$=3. With these same parameters, three specimens in double-lap configurations (DS20E30) were also tested to investigate the out-of-plane effect on the damage of the GFRP. The configuration S40E40 had $s/d$=4 and $e/d$=4. For two-bolt connections, two configurations were also tested. The geometric parameters considered were $s/d$=4, $e/d$=4 and $p/d$=3 for the configuration S40E40P30; $s/d$=4, $e/d$=4 and $p/d$=5 for the configuration S40E40P50. Three to seven specimens were tested for each configuration for a total 25 tests.

***Experimental setup and testing of the connections***

The tests were conducted up to failure of the joint in shear using a 500 kN hydraulic testing machine. As shown in Figure 2(b), the end connections were designed to make the loading axis to coincide with the interface of the two plates so that the bolts were mostly loaded in shear. Specimens were clamped by the grips of the testing machine at both ends. A tensile force was applied at the bottom end while the top end was fixed. The load was applied at the rate of 1 mm/min and the load and displacement were recorded by the control system of the testing machine.

***Tensile tests of the materials***

The GFRP plates were taken from Extren 500 series panels. Extren 500 is manufactured by Strongwell Corporation. According to the manufacturer, it is made of E-glass fibres and polyester resin. It is typically reinforced with 50% Continuous Strand Roving (CSR) and Continuous Strand Mat (CSM). The roving provides strength in longitudinal (pultrusion)

direction while the mat provides multi-directional strength properties [4]. Steel specimens were cut from 350W flat bars.

Tension tests of GFRP coupons were conducted according to ASTM Standards D3039 [41] for longitudinal and transversal tensile strength and ASTM D3518 [42] for in-plane shear strength. For grade 350W steel coupons, ASTM Standard A370 [43] was used. Specimens had uniform width for GFRP and reduced width in the gage length for steel. Strength was measured as specified by the appropriate testing standards. Strain was measured by an axial extensometer. Typical stress-strain curves for steel in tension and GFRP in longitudinal tension, transversal tension and in-plane shear are presented in Figure 3. As it can be observed, GFRP material behaves linearly up to brittle failure. Steel shows an elasto-plastic behaviour. The average measured properties of GFRP coupons are summarized in the first column of Table 2. The properties presented in the other columns of this table are those obtained by other authors and they will be used in the finite element analysis. For steel, the average ultimate tensile strength and average yield strength were approximately 540 MPa and 370 MPa respectively. ASTM A325 bolt was not tested. However, its nominal guaranteed tensile strength is 825 MPa and its nominal shear strength is 495 MPa considering the shear strength equals to 0.6 times the nominal tensile strength [44].

Considering the much higher stiffness of steel compared to GFRP, there was no deformation observed on the steel plates and on the A325 steel bolt until GFRP reached failure. Therefore, the observations given in this section are for GFRP plates only.

***Failure mode of one-bolt single-lap configurations.*** Figures 4(a) and 4(b) show the typical failure modes of S20E30 and S40E40 respectively. The failure mode of each tested specimen is presented in Table 3. As it can be observed in this table and these figures, the failure mode was not identical within the same configuration. For configuration S20E30 presented on Figure 4(a),

214 the three typical failure modes were net-section, shear and cleavage. As noted in Table 3,
215 cleavage was the predominant mode within the specimens of this configuration. Cleavage failure
216 was also observed on the three specimens with bolt loaded in double-lap configuration
217 (DS20E30). Suggesting that the varieties of failure mode observed in single-lap could be due to
218 the out-of-plane deformation. On the outer face of some single-lap specimens, washer
219 penetration into the top layer was observed. This damage was not seen in double-lap
220 configuration as the bolt eccentricity was restrained. On configuration S40E40 shear failure was
221 the predominant mode while one specimen (S40E40-4) show cleavage failure. These two typical
222 failure modes are presented in Figure 4(b). For some of these connections, the GFRP plate also
223 present additional cracks either along the main failure line or around the bolt-hole. On the outer
224 face of some GFRP specimens, damage of the top layer due to the out-of-plane deformation was
225 also observed on the free end edge (shear path). This damage was more pronounced on larger
226 specimen than on narrow ones. A typical case of this deformation is shown on specimen
227 S40E40-3 (Figure 4b).
228 ***Force-displacement curves of one-bolt single-lap connections.*** Figures 4(c) show the typical
229 force-displacement curves of single-lap S20E30 and S40E40. It is observed that the GFRP plates
230 behave linearly up to approximately 15 kN. Then the loads continue to increase, but with a
231 reduced stiffness up to the peak load. The reduction of the stiffness is probably due to the
232 reduction of the clamping pressure between the two plates during loading. The average peak load
233 is observed at approximately 41 kN for S20E30 and 48 kN for S40E40 for an average
234 displacement of 2.9 and 2.3 mm respectively. No relation between failure mode and peak load
235 was observed. After the peak load, the curve suddenly drops down to about 10 to 20 kN for
236 S20E30 and 20 to 30 kN for S40E40 suggesting a partial failure on the GFRP. From this point,
237 the GFRP undergoes a progressive failure. The displacement to which the complete failure

238 occurred is unknown because the tests were stopped at this stage as the maximum load was
239 achieved and load was less than 50% of the maximum value. However, as it can be observed in
240 Figure 4(c), some test results suggest that this displacement can exceed 5 mm. The typical force-
241 displacement curve of double-lap DS20E30 is also presented in Figure 4(c). It is observed that
242 restraining the eccentricity improves the joint stiffness, which is now similar to that of S40E40.
243 However, the displacement at which the peak load occurs is lower compared to S20E30. The
244 average peak load for DS20E30 is 43.4 kN. Compared to the average strength in S20E30 (41
245 kN), strength reduction associated to out-of-plane deformation is negligible probably due to the
246 short connection length (shear path). More experimental tests are necessary to investigate this
247 effect on connections with wider plate and/or longer shear path.
248 As depicted in Figure 4(c), there is a particularity with the curve of specimens S20E30-1. The
249 linear behaviour of this curve is interrupted at approximately 1 mm displacement and 20 kN
250 force. Here the progression of the load remains insignificant up to 2 mm displacement. Then, the
251 load increases up to a peak value of 40 kN and a displacement of 3.7 mm. This interruption of
252 the load growth was due to the displacement (slippage) of the bolt in the bolt-hole. This same
253 behavior was also observed on S20E30-3. To prevent this behavior in the specimens tested later,
254 special attention was given to joint tightening to ensure the contact between the bolt-hole and the
255 bolt in the loading direction. In summary, increasing *s/d* from 2 to 4 and *e/d* from 3 to 4, led to a
256 moderately higher connection strength. The joint eccentricity was found to have limited effect on
257 the connection strength when *s/d*=2 and *e/d*=3. However, doubling the shear plane improves the
258 joint stiffness.
259 ***Failure mode of two-bolt connections.*** The typical failure mode of two-bolt GFRP-steel single-
260 lap connections is presented in Figures 5. The inner and outer faces of the two bolts connection
261 are presented because the failure mode was not always the same on both faces of the same

specimen. For example, in Figure 5(a), while the inner face of specimen S40E40P30-1 shows signs of net-section failure in the lower row, the outer face in Figure 5(b) shows propagation of cracks around the two bolt-hole (block shear failure). Therefore, it is difficult to characterize this failure mode within the conventional types of failure presented in Figure 1. However, for specimens S40E40P30-2 shows cleavage failure on both faces. Shear failure is observed on specimens S40E40P30-4. However, propagation of cracks in the shear path has different patterns in the inner and the outer faces. On the inner face (Figure 5a), the cracks start from the lower row and propagate towards the top free end of the plate. On the outer face (Figure 5b), the cracks are limited around the two holes. Figures 5(c) and 5(d) present crack damages respectively in the inner and outer face of S40E40P50. Compared to S40E40P30, the failure modes were more consistent on both faces. With S40E40P50, shear failure was the predominant mode. Shear damage was in some cases limited around the bolt-hole (S40E40P50-3), while in other cases (S40E40P50-4) it started at the top row and propagated towards the free end of the plate. Other specimens fail in cleavage (S40E40P50-2). Here, cracks initiated on the side of the lower bolt-hole and propagated through the top bolt-hole and towards the free end distance. It was also noted that all these configurations show some bearing damage at the lower row. However, no complete bearing failure of the joint was observed.

The top layer of all single-lap configurations shows additional crack damages due to the out-of-plane deformation. In two bolt-column, the crack started at the lower row and propagated toward the top row but are interrupted by the compression induced on the washer of the top bolt. This compression forces the top layer of the GFRP plate to develop several cracks between the two bolt-hole as it can be observed on specimens S40E40P30-2, S40E40P50-3 and S40E40P50-4 (Figure 5b and 5d). This phenomenon can be observed in Figure 6(a). In one bolt single-lap, these crack damages freely propagated through the shear path as shown in Figure 4(b) for

specimen S40E40-3. It can also be noted that doubling the number of bolt did not change the failure mode. Shear and cleavage failures are the observed modes in one-bolt and two-bolt connections with $s/d$=4 and $e/d$=4. Observing cleavage failure in such long and wide connections is not surprising as this mode is typical to highly orthotropic composite material.

***Force-Displacement curves of two bolts connections.*** In Figure 6, the typical force-displacement curves of S40E40P30 and S40E40P50 are compared. The load history is similar to that observed with one-bolt joints. The peak loads are observed at 75 and 78 kN for S40E40P30 and S40E40P50 respectively. Hence, only 4% gain in the joint capacity was achieved by increasing the pitch. However, displacement at failure increased from an average of 2.1 mm for S40E40P30 to an average of 3.8 mm for S40E40P50. The loads sustained by the GFRP plates after the peak load were scattered and vary from 15 kN to 40 kN in both configurations. Therefore, increasing the pitch distance has no significant effect on the GFRP plate carrying capacity. Nevertheless, the joints with higher pitch distance were able to achieve more displacement, therefore a safer behavior. The typical force-displacement curve of S40E40 is also presented on Figure 6. It can be observed that increasing the number of bolts with a constant end-distance and side-distance ($e/d$=4 and $s/d$=4) from one bolt to two bolts in a column increased the joint capacity by approximately 60%. It is significant that increasing the number of bolts from one to two did not double the load capacity of the GFRP connection. It can also be observed that the peak load of the GFRP plate occurred at approximately the same displacement for S40E40 and S40E40P30.

In summary, the damage behavior of single-lap connection was difficult to assess. The incompatibility of stiffness between GFRP and steel plates could have been one of the contributing factors of the observed deformations. Using GFRP plate thicker or wider than steel plate could improve the joint stiffness. As carbon composites are stiffer, they might better

address the deformation issues in the composite part of the joints than glass composite. For this study, glass composite was selected instead of carbon composite due to its low cost and availability. Furthermore, with carbon composite, galvanic corrosion could occur and would need to be addressed.

## Comparison of experimental and predicted results

The ASCE Pre-standard [1] is the most recent design reference for GFRP in civil engineering application. For this analysis, the nominal strength prediction obtained using equations recommended by this ASCE Pre-standard [1] are compared with experimental test results of one-bolt and two-bolt connections. Since only the nominal strength is considered, no resistance factor is used for the calculation of the strength predictions.

***Design equations***

ASCE Pre-standard [1] provides equations corresponding to each potential failure mode. For net-section failure for a multi-row of bolts, it establishes net-section strength ($R_{nt}$) presented in Equation 1. The strength per bolt in configuration with one-row of bolt(s) is calculated using Equation 2.

$$R_{nt} = \left[\left(\frac{1}{\left(\frac{w}{nd}-1\right)}\left(1 + C_{Lt}\left(S_{pr} - 1.5\frac{S_{pr}-1}{S_{pr}+1}\theta\right)\right)L_{br}\frac{w}{nd}\right) + \left(\frac{\left[1+C_{op}\left(1+\left(1-1/S_{pr}\right)^{3}\right)\right](1-L_{br})}{1-n\frac{d_h}{w}}\right)\right]^{-1} w.t.f_{uLt} \quad (1)$$

$$R_{nt} = \left[1 + C_{Lt}\left(S_{pr} - 1.5\frac{S_{pr}-1}{S_{pr}+1}\theta\right)\right]^{-1}(w - n.d_h)t.f_{uLt} \quad (2)$$

with:

$$\theta = 1.5 - 0.5\left(\frac{e}{w}\right) \text{ and } S_{pr} = w/d \text{ for one-bolt per row}$$

$$\theta = 1.5 - 0.5\left(\frac{e}{g}\right) \text{ and } S_{pr} = g/d \text{ for multi-bolt per row}$$

$C_{Lt}$=0.4 for plate and $C_{op}$=0.5 for shape.

$L_{br}$ is the proportion of the connection force taken in bearing at the first bolt row (see Figure 2a). The value of $L_{br}$ can be found in [1],

$f_{uLt}$ is the tensile strength in the longitudinal direction of the GFRP plate,

n is the number of bolts in a row.

The nominal shear tear-out strength ($R_{sh}$) per bolt for connection with one-row of bolt(s) is defined in Equation 3. Equation 4 gives the shear tear-out strength per column of bolts for connection with two rows of bolts separated by a pitch ($p$).

$$R_{sh} = 1.4\left(e - \frac{d_h}{2}\right) t.f_{ipsh} \quad (3)$$

$$R_{sh} = 1.4\left(e - \frac{d_h}{2} + p\right) t.f_{ipsh} \quad (4)$$

Where $f_{ipsh}$ is the characteristic in-plane shear strength of the GFRP plate.

The bearing strength ($R_{br}$) per bolt is the product of bearing area to the bearing strength ($f_{br}$) of the material as defined in Equation 5.

$$R_{br} = t.d.f_{br} \quad (5)$$

For single bolt centrally positioned with $e/d < 4d$, cleavage strength ($R_{cl}$) is the lesser of Equations 6 and 7.

$$R_{cl} = 0.15\left((2.s - d_h)f_{uLt} + 2.e.f_{ipsh}\right).t \quad (6)$$

$$R_{cl} = \left(\frac{10}{9} - \frac{4}{9}\frac{d_h}{e}\right)^2 t.d.f_{br} \quad (7)$$

Since $f_{br}$ was not tested in the present experimental study, the ratio of $f_{br}/f_{uLt}$ =1.8 measured by Rosner and Rizkalla [10] was taken.

For a single-row of bolts (with the maximum number of bolts in the row set to three) at uniform gage distance ($g$), cleavage strength ($R_{cl}$) is defined as:

$$R_{cl} = 0.15\left((2.s + 0.5g - d_h)f_{uLt} + 2.e.f_{ipsh}\right).t \quad (8)$$

Cleavage strength prediction is not provided for a multi-row of bolts in the ASCE Pre-standard [1]. For connection with multi-row of bolts, ASCE Pre-standard [1] also recommends multiplying the nominal strength of the connection by the ratio of $p/4d$ when $p/d < 4$.

***Analysis of the predicted results***

In Table 4, columns 4 to 8 list the results obtained using Equations 1 to 7. The average tensile strengths obtained from the tested coupons and reported in Table 2 were used in the calculation. The governing failure load and failure mode are reported in columns 9 and 10. The predicted to experimental ratios are also reported in column 11.

For connection S20E30, experimental study produced three types of failure mode: net-section, shear tear-out and cleavage failures. However, among the seven specimens tested for this configuration, failure by cleavage was the predominant mode while only cleavage failure was observed for DS40E30. The ASCE Pre-standard [1] predicts that cleavage governs design, which is consistent with some experimental specimens. However, the predicted strength governed by Equation 6 was underestimated by 53% to 55%. For connection S40E40, failure by shear was the predominant mode observed experimentally. The ASCE Pre-standard [1] predicts that failure by shear governs the design. However, it underestimates the strength by 15% compared to experimental tested results. It is important to note that the ASCE Pre-standard [1] recommends that cleavage should not be considered for connection with $e/d \geq 4$. However, experimental results reveal that this failure mode is possible for $e/d=4$.

The ASCE Pre-standard [1] predicts net-section failure for S40E40P30 and S40E40P50. It was rather shear tear-out and cleavage that were observed experimentally for S40E40P30. Shear tear-out was also the predominant failure mode observed experimentally for S40E40P50. Therefore, the predicted failure mode is not consistent with experimental observations. While the strength prediction of S40E40P50 is only 18% below the experimental failure load, that of S40E40P30 is

underestimated by 36%. For S40E40P30, this larger underestimation is due to the requirement of multiplying the net-section connection strength by the ratio of $p/4d$ when $p$ is less than the required minimum. Such recommendation significantly reduced the connection strength prediction even though it was observed experimentally that the pitch had limited effect on the failure load. ASCE Pre-standard [1] does not provide an equation of cleavage strength for multi-row of bolts. However, in experimental section, some specimens of S40E40P30 and S40E04P50 show failure by cleavage. Therefore, it could be useful to define an equation capable of predicting this failure mode for a multi-row of bolts.

More data are required to better understand the relationship between the different geometric parameters and the connection strength. Finite element approach will be used to extend such data.

## Finite element analysis

### *Overview of the finite element analysis*

Through FE analysis, this section aims to investigate the effects of the end-distance ($e$), the side-distance ($s$) and the pitch ($p$) on the connection strength. A two-dimensional (2D) finite element model was developed with the commercial software ADINA 8.7.3. The analysis started with a validation study based on experimental results described above and also with the data of some papers discussed above [10, 17]. The properties shown in Table 2 were used for this part of the study. This validation was followed by a parametric simulation where the effect of geometrical parameters for one-bolt connections and two-bolt connections aligned parallel to the loading direction, was investigated. The ratio were $1 \leq e/d \leq 5$ and $1.5 \leq e/d \leq 5$. The pitch-distance ($p/d$=2, 3, 4 and 5) for two-bolt parallel to the loading direction (two-bolt in a column) were also investigated. In the parametric study, two types of GFRP plates were studied: one with the ratio of $E_{Tt}/E_{Lt}$=0.2 using the properties of the plates in the current study; the other with the ratio of $E_{Tt}/E_{Lt}$=08 using the properties of the plates reported by [17]. The interest the two types of plates

is the relative proportion of CSR and CSM. The model with $E_{Tt}/E_{Lt}$=0.2 represents a highly orthotropic material. It achieves higher strength in the pultruded direction than in the transversal direction. On the other hand, with a ratio of $E_{Tt}/E_{Lt}$ =0.8, the relative proportion of CSM and CSR leads to quasi-isotropic plate.

***Analysis assumptions***

This study was limited to the evaluation of joint strength and failure mode for GFRP with loading parallel to the pultruded direction. In the experimental study of GFRP-to-steel connection, failure of the joint was due to the GFRP fracture. Therefore, only the GFRP plate was modelled in the finite element (FE) analysis. Figure 7(a) presents the typical 2D model used for this analysis. For model validation, all configurations tested in the experimental program were analysed. Additional configurations reported in others papers [10; 17] were also used. Their material properties are presented in Table 2 while details of chosen configurations are presented in Table 5. In the static environment of ADINA, the GFRP plate was modelled as a 2D solid with a quadrilateral element. These elements haves nine nodes per element and six degrees of freedom per node. The mesh density is shown in Figure 7(a). Each element edge length was approximatively equal to 2 mm. The mesh density was refined around the bolt-hole. In a square refined mesh area, the length ratio of the element edges (last element/first element) was equal to 0.2. It was verified that further reducing the mesh size does not influence the stress distribution in the model. The GFRP plate was modelled as a plastic orthotropic material. The anisotropy parameters were determined from yield stresses. The input yield stresses were taken as the ultimate tensile strengths of the material and the input plastic strain was taken as a material longitudinal tensile strain. Contact between the bolt and the plate was modelled by a contact feature available in ADINA. To reduce the computation time, the bolt was modelled as a rigid half cylinder. The contact interface was generated as a pair of surface elements. On this interface,

426 the bolt was defined as a target surface and the bolt-hole elements as a contactor surface. This
427 assumption was based on the fact that the elastic modulus of the steel bolt is greater than that of
428 GFRP plate. Due to the use of contact elements, no boundary condition was applied on this
429 interface. For all configurations, the length L presented in Figure 7(a) was always constant and
430 equal to 127 mm. A uniform pressure was applied in the longitudinal Z-axis on the far end plate
431 edge. The external load was applied incrementally on the structure. Once the GFRP plate reached
432 the input strain, the model diverged. The recorded peak load was taken as the strength of the
433 connection.

434 ***Validation of the finite element model***

435 Figures 7(b) to 7(g) present the post-processing Hill effective stress distribution of the FE model.
436 Based on the stress distribution along a given failure path of the model, the joint failure mode
437 was defined. For example, for shear tear-out failure presented in Figure 7(b) and 7(c), excessive
438 stresses are developed between the sides of the bolt-hole and propagate towards the free end
439 edge of the plate. For net-section failure, excessive stresses are developed across the centerline of
440 the bolt-hole in the net-section path (Figure 7d). A typical bearing failure is presented in Figure
441 7(e); stresses are limited ahead of the bolt-hole in the bearing path and barely reach the free end
442 edge of the plate. Cleavage failure is characterized by excessive stresses ahead of the bolt-hole
443 (Figure 7f) In addition, excessive stresses also develop from the free end edge of the plate
444 towards the bolt-hole in the loading direction. In Table 5, the ultimate loads ($P_{FE}$) and failure
445 modes obtained from FE analysis of one and two bolts connections are compared to the average
446 experimental failure loads. It can be observed that the FE results are in very good agreement with
447 experimental results. In general, the FE failure loads are slightly conservative. All ratios of
448 predicted to experimental results are within 8% difference. The observed FE failure modes were
449 also quite consistent with the experimental failure modes. In Figure 8, the typical force-

displacement curves obtained in the FE analysis are compared to that of experimental results. Here also, it can be seen that the force-displacement history are quite consistent with that of experimental curves up to the peak load at which the FE model stops.

**Parametric simulation and analysis of the results**

Following the satisfactory agreement between FE model and experimental results, a parametric study was carried out. The results obtained from the parametric simulation are presented in Table 6. For connections with one or two bolts, the FE results were used to define the boundaries of predicted failure modes and are shown in Figure 9 by dashed lines. These boundaries are presented in Figure 9(a) for one-bolt connections of GFRP plates with $E_{Tt}/E_{Lt}$=0.2 and in Figure 9(b) for those with $E_{Tt}/E_{Lt}$=0.8. The boundaries of predicted failure modes according to ASCE Pre-standard [1] were also identified and are shown by the lines in Figure 9(c) for connections of a GFRP plate with $E_{Tt}/E_{Lt}$=0.2, and in Figure 9(d) for $E_{Tt}/E_{Lt}$=0.8. Failure modes from our experimental study and those reported in reference papers are listed in Table 7. They are represented by symbols in Figure 9 where they are regrouped for $E_{Tt}/E_{Lt}\leq$0.3 in Figures 9(a) and 9(c) or $E_{Tt}/E_{Lt}\geq$0.7 in Figures 9(b) and 9(d). Failure loads from Table 6 are reported in Figures 10(a) and 10(b) for various geometrical parameters of one-bolt connections. The predicted failure loads using ASCE Pre-standard [1] for the minimum recommended side-distance are also shown by the dotted line. The numbers in parenthesis in Figure 10 identify the equation that governs the design according to [1] with the minimum recommended side-distance ($s/d$=1.5). For two-bolt connections, information similar to Figure 9 and 10 is provided in Figures 11 and 12.

***Effects of geometric parameters in one-bolt connections***

For one-bolt connection, FE results in Figures 9(a) and 9(b) identified three failure zones: cleavage, shear and net-section for connections with highly orthotropic GFRP plates and cleavage, net-section and bearing for those with quasi-isotropic GFRP plates. On the other hand,

ASCE Prestandard [1] identifies the fours failure zones for each material. The experimental data points presented in Figure 9(b) and 9(c) show that FE analysis provided better predictions than [1] for connections with quasi-isotropic GFRP plates. However, due to the limitted number of data point, it is difficult to conclude which one of the FE analysis or the ASCE Pre-standard equations provide the best predictions for these failure modes in the case of a highly orthotropic plate. Therefore, more experimental data points would be needed for this material.

The failure loads predicted by FE analysis for one-bolt connections are presented in Table 6. For connections with $E_{Tt}/E_{Lt}$=0.2 and $E_{Tt}/E_{Lt}$=0.8, it can be observed that for $s/d \leq 1.5$, there is no significant gain in failure load when $e/d > 4$. Similarly, for $s/d \geq 2$, there is no increase in failure load when $e/d > 4$. It is useful to compare this observation with ASCE Pre-standard [1] or manufacturer [4,6] recommendations. For one-bolt connection, ASCE Pre-standard [1] recommends the minimum values of $e/d$=4 and $s/d$=1.5. This appears to be a conservative geometrical value for the end-distance since the FE analysis shows that approximately the same failure load can be attained for $s/d$=1.5 and $e/d$=3. On the other hand, the manufacturers recommend a minimum combination of $e/d$=3 and $s/d$=2. For these parameters, the FE predicted load is approximately 55% higher than the one corresponding to the recommendation of ASCE Pre-standard [1] for both materials.

All FE values associated to one-bolt connections are illustrated in Figures 10(a) and 10(b). The prediction of ASCE Pre-standard [1] for the minimum recommended side-distance $s/d$=1.5 is identified by the dotted line in these figures. When comparing the FE predictions and ASCE Pre-standard [1] predictions for $s/d$=1.5 (Figure 10a), the strengths predicted by [1] governed by cleavage (equation 6) are approximately 50% lower than FE analysis that also predcits cleavage for $e/d$=2 and $e/d$=3. However, for all other values of $e/d$, the loads predicted by [1] are consistent with the FE predicted loads. For connections of quasi-isotropic GFRP plates

presented in Figure 10(b), the failure loads predicted by [1] for $s/d$=1.5 and varying values of $e/d$ are all quite consitent with the FE predicted loads. Although predicted loads with ASCE Pre-standard [1] are governed by the same design equations as for highly orthotropic plates, cleavage strength predicted using Equation 6 seems to provide a better prediction for quasi-isotropic than for highly orthotropic plates.

***Effects of geometric parameters in two-bolt connections***

For two-bolt connection, FE results in Figures 9(a) and 9(b) identifies three failure zones: cleavage, shear and net-section for connections with highly orthotropic GFRP plates. For connections with quasi-isotropic GFRP plates, only two failure zones: cleavage and net-section are identified. On the other hand, ASCE Prestandard [1] identifies only shear and cleavage zones for connections with highly orthotropic GFRP plates and net-section failure is the only occuring mode for those with quasi-isotropic GFRP plates. The experimental data points presented in Figure 11(b) and 11(d) show that FE analysis provided a better predictions than [1] for connections with quasi-isotropic GFRP plates. However, the limit number of data points for highly orthotropic plate is not sufficient to conclude on the actual predictions. Therefore, more experimental data points would be needed for this material.

The failures loads predicted by FE analysis for two-bolt connections are presented in Table 6. For connections of highly orthotropic plates with $E_{Tt}/E_{Lt}$=0.2, it can be observed that for $s/d$=1.5, there is no significant gain in failure load when $e/d>2$. Similarly, for $s/d\geq2$, there is no significant increase in failure load when $e/d\geq4$. For connections of quasi-isotropic plates with $E_{Tt}/E_{Lt}$=0.8, no significant increase in the failure load is observed when $e/d\geq2$ and $s/d\leq3$. Above $s/d>3$, the strength increases with $e/d$ up to a ratio of 3. It is useful to compare this observation with ASCE Pre-standard [1] or manufacturer [4,6] recommendations. For two-bolt connection, ASCE Pre-standard [1] recommends the minimum values of $e/d$=2, $s/d$=1.5 and $p/d$=4. On the

other hand, the manufacturers recommend a minimum combination of $e/d$=3, $s/d$=2 and $p/d$=3. The recommendation of the manufacturer leads to a connection strength approximately 52% and 57% higher than that corresponding to the ASCE Pre-standard [1] minimum values for connections with $E_{Tt}/E_{Lt}$=0.2 and $E_{Tt}/E_{Lt}$=0.8 respectively. It is interresting to note that, for all values associated to two-bolt connections in Table 6 increasing $p/d$ above 3 has little effect on the connection failure load.

The FE values associated to two-bolt connections are also illustrated in Figure 12(a) and 12(b) for the recommended value of $e/d$=2 with various ratios of $s/d$ and $p/d$. The prediction of ASCE Pre-standard [1] for the minimum recommended side-distance $s/d$=1.5 is identified by the dotted line in these figures. When comparing the FE predictions and ASCE Pre-standard [1] predictions for $s/d$=1.5, the difference in prediction is significant for values of $p/d$<4 for both types of plates. For these geometric parameters, the design values are governed by net-section failure (Equation 1) which produces the predicted strengths approximately 60% lower than FE prediction for $p/d$=2 and 38% for $p/d$=3 for highly orthotropic plates. For quasi-isotropic plates this difference is 38% for $p/d$=2 and 26% for $p/d$=3. However, when $p/d\geq$4, the results predicted by [1] are quite consistent with FE results. In that case, the maximum difference between the predicted loads and the FE loads is nearly 17% for connections with $E_{Tt}/E_{Lt}$=0.2 while it does not exceed 16% for connections with $E_{Tt}/E_{Lt}$=0.8. This larger difference for values of $p/d$<4 is due to the recommendation of ASCE Pre-standard [1] to reduce the predicted strength of connection with $p/d$<4 to the ratio of $p/4d$.

## CONCLUSIONS

544 The aim of this paper was to investigate the effect of geometric parameters and material
545 properties on the behavior of GFRP-to-steel bolted connections. An experimental study on a
546 GFRP pultruded plate connected to a steel plate was performed. The effects of increasing the
547 side-distance, the end-distance, the pitch, and the number of bolts in the joint were discussed.
548 The experimental results were compared to the strength calculated from ASCE Pre-standard [1].
549 Finally, FE analysis along with experimental data, were used to evaluate the failure load and
550 failure mode of other geometric parameters. It was found that:

551 • The parametric study showed that the failure mode can be better predicted with the FE
552 model than with ASCE Pre-standard [1] for both highly orthotropic and quasi-isotropic
553 materials.

554 • For one-bolt connection, the experimental results obtained in the present study show that
555 increasing *s/d* from 2 to 4 and *e/d* from 3 to 4, lead to a moderately higher strength and an
556 improved behavior of the joint at failure. Bearing failure was not observed due to the use
557 of highly orthotropic material. Experimental data along with FE parametric analysis show
558 that this failure mode would happen for GFRP plate with quasi-isotropic material.

559 • For two bolt in a column, the experimental results show that increasing the pitch distance
560 from 3 to 5 provides no significant increase of capacity. Nevertheless, the connections
561 with higher pitch distance were able to achieve more displacement, therefore a safer
562 behavior. The experimental data and FE analysis reveal that pure bearing failure is not
563 likely to occur. For connections with highly orthotropic plate, shear or cleavage were
564 found to be the predominant failure modes. For connections with quasi-isotropic plates,
565 cleavage was observed for short end-distance and net-section failure was predominant for
566 $e/d>2$.

- The out-of-plane deformation was found to have limited effect on the strength of the tested connections (S20E30). Failure modes in single-lap were difficult to assess as a variety of failure modes were observed within the specimens of the same configurations or within the outer and inner faces of the same specimen. This variety of failure modes was not observed in the double-lap configuration.
- ASCE Pre-standard [1] does not always predicts failure modes that are consistent with experimental observations. The strength predicted by ASCE Pre-standard [1] is too conservative for some configurations.

## RECOMMENDATION

Based on the results of this work, recommendations to improve the ASCE Pre-standard [1] are formulated as follows.

- The values of $s/d$=2 and $e/d$=3 should be considered as a minimum values for GFRP bolted connections as they were found to provide higher strength than the strength obtained with the values recommended by ASCE Pre-standard [1].
- The recommendation of ASCE Pre-standard [1] to multiply the connection strength by the ratio of $p/4d$ when $p$ is less than the required minimum could significantly underestimate the strength of the connection for both highly orthotropic and quasi-isotropic materials. Therefore, further consideration should be given to this aspect.
- More experimental data especially for connections with highly orthotropic GFRP plate ($E_{Tt}/E_{Lt} \leq 0.3$) are required to validate some of the parametric observations. For quasi-isotropic GFRP plate ($E_{Tt}/E_{Lt} \geq 0.7$), additional experimental data will be necessary to define the bearing failure mode zone.
- More experimental analyses are necessary to study the effect of out-of-plane deformation on multi-row bolts.

## ACKNOWLEDGEMENTS

The financial support provided by Natural Science and Engineering Research Council of Canada (NSERC) is well appreciated. Special thanks to the manufacturer Strongwell Corporation for providing GFRP plates.

## REFERENCES

[1] ASCE. *Pre-Standard for Load and Resistance Factor Design (LRFD) of Pultruded Reinforced Polymer structure (Final)*. USA, 2010, pp.67-84.

[2] Clarke J.L. *EUROCOMP Design Code and Handbook*. London. E & FN Spon. First Edition, 1996, ISBN 0 419 19450 9

[3] CNR-DT 205/2007. *Guide for the Design and Construction of Structures Made of FRP Pultruded Elements*. Advisory Committee on Technical Recommendation for Construction. http://www.cnr.it/documenti/norme/IstruzioniCNR_DT205_2007_eng.pdf

[4] Strongwell. *Extren Design Manual*, Bristol, VA, 2002.

[5] Fiberline Composites. *The Fibreline Design Manual*. Denmark, 2003.

[6] Creative Pultrusions. *The Pultex Pultrusion Global Design Manual*. Alum Bank, PA, 2001.

[7] Bank, L.C. *Composite for Construction Structural Design with FRP materials*. John Wiley & Sons, Inc. USA, 2006.

[8] Thoppul S.D., Finegan J. and Gibson R.F. Mechanics of mechanically fastened joints in polymer-matrix composite structures - A review, Composites Science and Technology 2008; 69:301-329.

[9] Mottram JT. and Turvey GJ. Physical test data for the appraisal of design prcedures for bolted joints in pultruded FRP structural shapes and systems, Progress in Structural Engineerong and Materials 2003; 5(4): 195-222.

[10] Girao Coelho AM. and Mottram JT. A review of the behaviour and analysis of bolted connections and joints in pultruded fibre reinforced polymers, Materials and Design, 2015; 74: 86-107.

[11] Mottram JT. Reference and bibliography database on research and development with pultruded fibre reinforced polymer shapes and systems, 2014. http://www2.warwick.ac.uk/fac/sci/eng/staff/jtm/prfp_latest.pdf

[12] Abd-El-Naby S.F.M. and Hollaway L. The experimental behaviour of bolted joints in pultruded glass/polyester material. Part 1: Single-bolt joints. Composites 1993a, 24(7): 531–538.

[13] Rosner C.N. and Rizkalla S.H. Bolted connections for fibre-reinforced composite structural members: Experimental program. Journal of Materials in Civil Engineering, ASCE 1995, 7(4): 223–231.

[14] Erki M.A. Bolted glass-fibre-reinforced plastic joints. Canadian Journal of Civil Engineering 1995; 22: 736–744.

[15] Cooper C. and Turvey G.J. Effects of joint geometry and bolt torque on the structural performance of single bolt tension joints in pultruded GRP sheet material. Composite Structures, 1995, 32(1–4): 217–226.

[16] Yuan, R.L., Liu, C.J., and Daley, T. Study of mechanical connection for GFRP laminated structures, *Proc. 2nd International Conference on Advanced Composite Materials in Bridges*

635 *and Structures ACMBS*-2, The Canadian Society for Civil Engineers, Whistler, 1996, 951-
636 958.
637 [17] Ramaskrishna S. Hamada H. and Nishiwaki M. Bolted joints of pultruded sandwich
638 composite laminates. Composite Structures 1995; 32: 227-235
639 [18] Yuan, R.L. and Weyant, S.E. The effect of environmental exposure of the behavior of
640 pultruded mechanical connections, *in Proc. Annual Conf. Composite Institute, SPI*, 1997,
641 Session 14-F.
642 [19] Turvey, G.J. Single-bolt tension joint tests on pultruded GRP plate: effects of tension
643 direction relative to pultrusion direction, Compos. Struct., 1998, 42(4), 341-351. DOI:
644 10.1016/S0263-8223(98)00079-8
645 [20] Yuan, R.L., and Liu, C.J. "Experimental characterization of FRP mechanical connections",
646 *Proc. 3rd International Conference on Advanced Composite Materials in Bridges and*
647 *Structures ACMBS*-3, The Canadian Society for Civil Engineers Montreal, 2000, 103–110.
648 [21] Turvey, G.J. and Wang, P. Single-bolt tension joints in pultruded GRP material Effect of
649 temperature on failure loads and strengths and joint efficiency, *in Proc. Conf. on Strain*
650 *Measurement in the 21st Century, British Society for Strain Measurement*, 2001, 20-23.
651 [22] Turvey, G.J. and Wang, P., 'Effect of temperature on the structural integrity of bolted joints
652 in pultrusions,' *in Proc. Inter. Conf. on Composites in Construction – CCC2001*, A.A.
653 Balkema Publishers, (Swets & Zeitlinger) Lisse, 2001, 171-176.
654 [23] Wang, Y. Bearing behavior of joints in pultruded composites, J. Compos. Mater., 36(18),
655 2002, 2199-2216. DOI: 10.1177/0021998302036018535
656 [24] Turvey, G.J. and Wang, P. Single-bolt tension joints in pultruded GRP plate – effects of
657 elevated temperature on failure loads, failure modes, load orientation and joint efficiency, *in*
658 *Proc. Joining Plastics 2006, Rapra Conf. Proc*., 2006, Paper No. 9.
659 [25] Turvey, G.J. and Wang, P., Thermal preconditioning study for bolted tension joints in
660 pultruded GRP plate, Composite Structures, 77 4, 2007, 509-513.
661 [26] Turvey, G.J. and Wang, P., Failure of pultruded GRP single-bolt tension joints under hot–
662 wet conditions, Composite Structures, 77 4, 2007, 514-520.
663 [27] Turvey, G.J. and Wang, P., Effect of hole clearance on bolt loads in pultruded GRP tension
664 joints, *in Proc. 16th Inter. Conf. on Composite Materials (ICCM-16)*, July 2007, Kyoyto.
665 [28] Turvey G.J. and Wang, P., Failure of pultruded GRP bolted joints: a Taguchi analysis,
666 Engineering and Computational Mechanics, 162 3, 2009, 155 –166
667 [29] Turvey, G.J., Failure of single-lap single-bolt tension joints in pultruded glass fibre
668 reinforced plate, *Proc. 6th International Conference on Composites in Construction*
669 *Engineering (CICE)*, Rome, 2012, Paper 08.089.
670 [30] Turvey, G.J. and Godé, J. An experimental investigation of the tensile behaviour of single-
671 lap bolted joints in pultruded GFRP plate, *in Proc. of FRP Bridge Conf.*, London, Net
672 Composites, Chesterfield, 2012, 77-91. CD-ROM
673 [31] Zafari, B. and Mottram, J.T., Effect of hot-wet aging on the pin-bearing strength of a
674 pultruded material with polyester matrix, J. of Composites for Construction, 16 3, 2012, 340-
675 352.
676 [32] Turvey, G.J., Ultimate loads, strength, extensions and strains of pultruded GFRP single-lap,
677 single-bolt tension joints, *in Proc. 6th Inter. Conf. on Advanced Composites in Construction*,
678 Net Composites Ltd., Chesterfield, UK, 2013, 373-382.
679 [33] Lee, Y-G., Choi, E. and Yoon, S-J, Effect of geometric parameters on the mechanical
680 behavior of PFRP single bolted connection, Composites Part B –Engineering, 75, 2015, 1-10.
681

[34] Abd-El-Naby S.F.M. and Hollaway L. The experimental behaviour of bolted joints in pultruded glass/polyester material. Part 2: two-bolt joints. Composites 1993b, 24(7): 539–546.
[35] Prabhakaran R., Devara S. and Razzaq Z. The effect of fiber orientation angle on the unnotched, open hole, and pin-loaded strength of a pultruded composite. In: *Proceeding of the 51st Annual Conference of the composite Inst. Society of the Plastic Industry*, Washington DC; 1996; 1-15.
[36] Prabhakaran R., Razzaq Z. and Devara S. Load and resistance factor design (LRFD) approach for bolted joints in pultruded composites. Composites Part B: Engineering 1996; 27: 351–360.
[37] Hassan N.K., Mohamedien M.A. and Rizkalla S.H. Multibolted joints for GFRP structural members. Journal of Composites for Construction, ASCE 1997; 1(1): 3-6.
[38] Prabhakaran, R., and Robertson, J., 1998, An experimental investigation of load-sharing in a multi-bolt pultruded composite joint, *Proc. 2nd International Conference on Composites in Infrastructure ICCI*, H. Saadatmanesh, M.R. Ehsani (eds.), Tucson, pp. 355-368.
[39] Turvey, G.J. and Wang P., Environmental effects on the failure of GRP multi-bolt joints, Structures and Buildings, 162 4, 2009, 275-287.
[40] Girão Coelho, A.M., Mottram J.T. and Harries, K.A., Bolted connections of pultruded GFRP: Implications of geometric characteristics on net section failure, Composite Structures, 131, (2015), 878-884.
http://dx.doi.org/10.1016/j.compstruct.2015.06.048
[41] ASTM D3039/D3039M-00:2006. Standard Test Method for Tensile Properties of Polymer–Matrix Composite Materials. Vol. 15.03. Composite Materials. ASTM International West Conshohocken, PA.
[42] ASTM D3518/D3518M-94:2007. Standard Test Method for In-Plane Shear Response of Polymer Matrix Composite Materials by Tensile Test of a ±45° Laminate–Matrix. Vol. 15.03. Composite Materials. ASTM International. West Conshohocken, PA.
[43] ASTM A370-12:2005. Standard Test Methods and Definitions for Mechanical Testing of Steel Products Vol. 01.03. ASTM International. West Conshohocken, PA.
[44] Kulak, G. L., Adams, P.F., Gilmor, M.I. *Limit States Design in Structural Steel*. Canadian Institute of Steel Construction, 5th edition, 1998.
.

## List of Figures

**Figure 1**. Failure modes: (a) Bearing, (b) net-section, (c) shear tear-out, (d) Block shear (e) cleavage

**Figure 2.** (a) Typical joint geometric parameters, (b) Test set-up

**Figure 3**. Stress-strain relationships of the materials

**Figure 4.** Typical failure damages of GFRP (a) Inner face S20E30, (b) Outer face S40E40, (c) Typical force-displacement curves of S20E30 compared to S40E40 and DS20E30

**Figure 5.** Failure damages of GFRP (a) Inner face of S40E40P30 (b) Outer face of S40E40P30, (c) Inner face of S40E40P50 (d) Outer face of S40E40P50.

**Figure 6.** (a) Out-of-plane deformation of a two bolt-column, (b) Typical force-displacement curves of S40E40P30 compared to S40E40P50 and S40E40.

**Figure 7.** (a) Typical 2D model, Post-processing failure modes: (b) bearing, (c) net-section, (d) and (e) shear tear-out, (f) cleavage.

**Figure 8**. Typical force-displacement curves of the experimental compared to finite element models: (a) S20E30, (b) S40E40, (c) S40E40P3, (d) S40E40P50.

**Figure 9.** Effect of *e/d* and *s/d* on failure modes for one-bolt: (a) FE and Exp. failure modes for highly orthotropic plates; (b) FE and Exp. failure modes for quasi-isotropic plates; (c) [1] and Exp. failure modes for highly orthotropic plates; (d) [1] and Exp. failure modes for quasi-isotropic plates;

**Figure 10.** Effect of *e/d* and *s/d* on joint strength for one-bolt: (a) FE failure loads for highly orthotropic plates; (b) FE failure loads for quasi-isotropic plates

**Figure 11**. Effect of geometric parameters on failure modes for two-bolt: (a) FE and Exp. failure modes for highly orthotropic plates; (b) FE and Exp. failure modes for quasi-isotropic plates; (c) [1] and Exp. failure modes for highly orthotropic plates; (d) [1] and Exp. failure modes for quasi-isotropic plates

**Figure 12**. Effect of geometric parameters on joint strength for two-bolt: (a) FE failure loads for highly orthotropic plates; (b) FE failure loads for quasi-isotropic plates

## List of Tables

Table 1. Minimum geometric requirements from design manuals (*d*: diameter of the bolt, $d_h$:

755

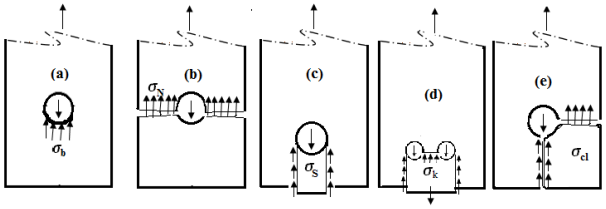


**Figure 1**. Failure modes: (a) Bearing, (b) net-section, (c) shear tear-out, (d) Block shear (e) cleavage

756
757
758
759

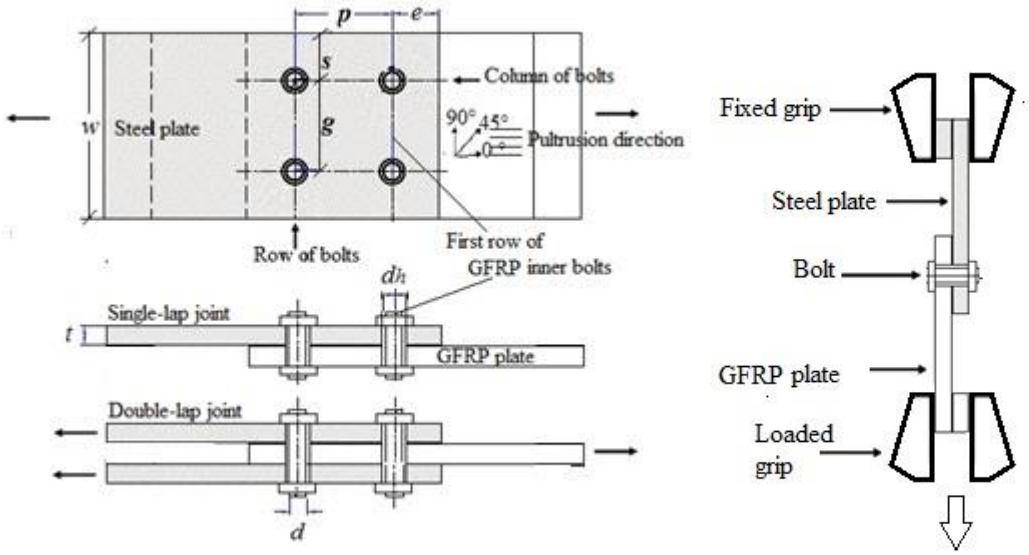


**Figure 2.** (a) Typical joint geometric parameters, (b) Test set-up

760

761

762

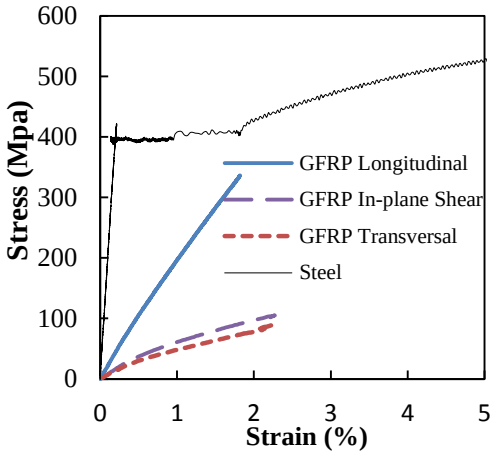


**Figure 3**. Stress-strain relationships of the materials

763

764

765

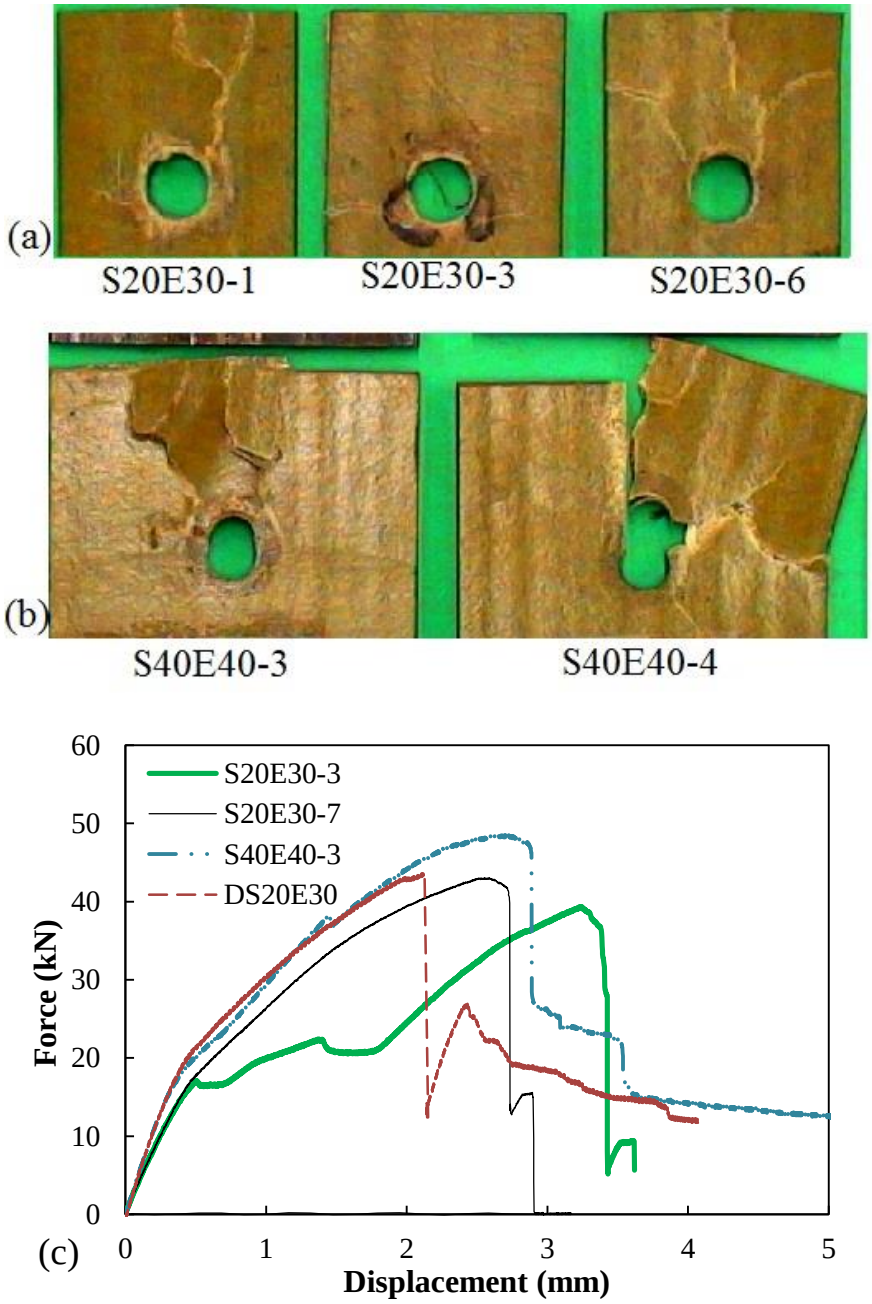


**Figure 4.** Typical failure damages of GFRP (a) Inner face S20E30, (b) Outer face S40E40, (c) Typical force-displacement curves of S20E30 compared to S40E40 and DS20E30

766

767

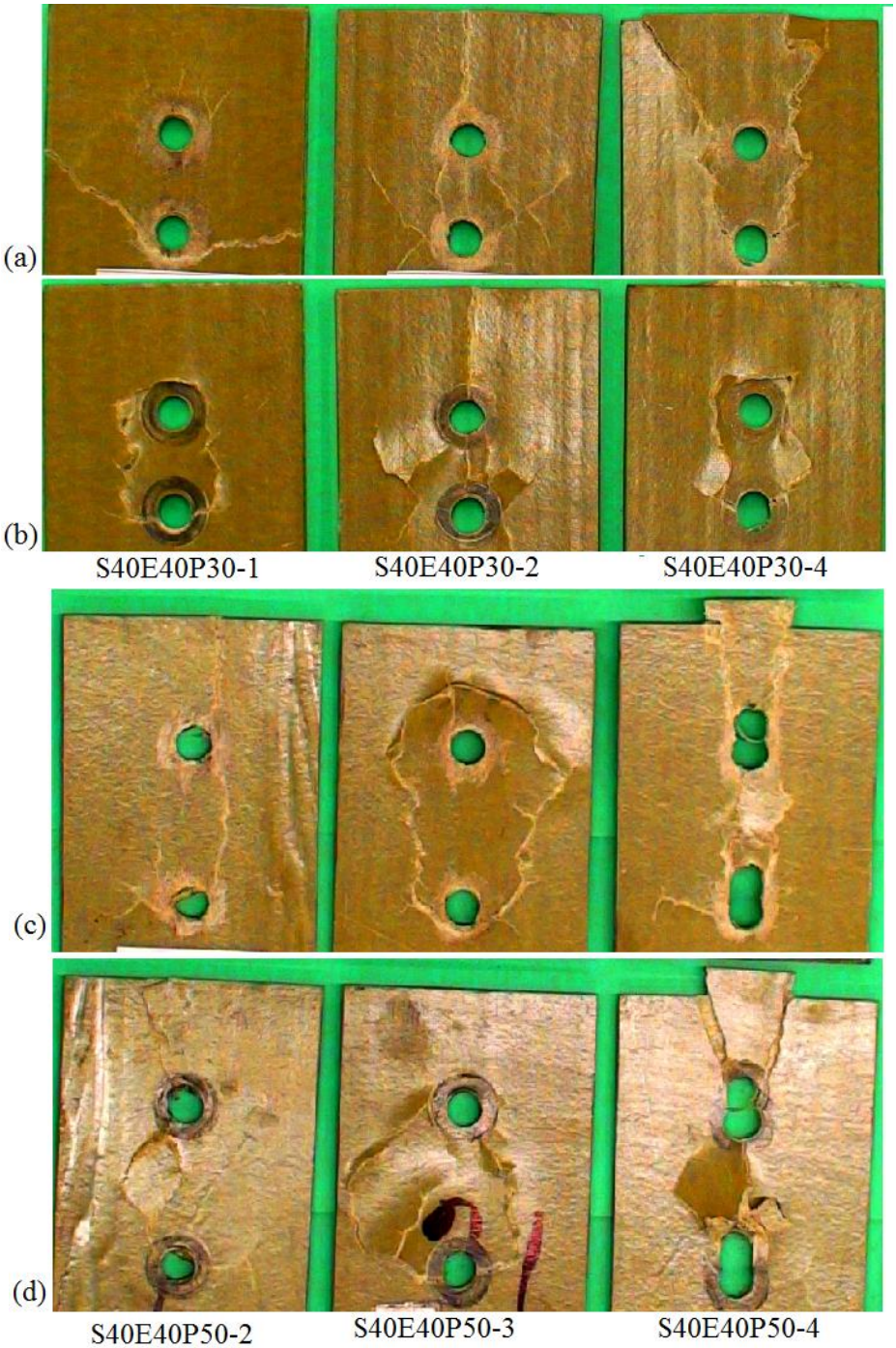


**Figure 5.** Failure damages of GFRP (a) Inner face of S40E40P30 (b) Outer face of S40E40P30, (c) Inner face of S40E40P50 (d) Outer face of S40E40P50.

768

769

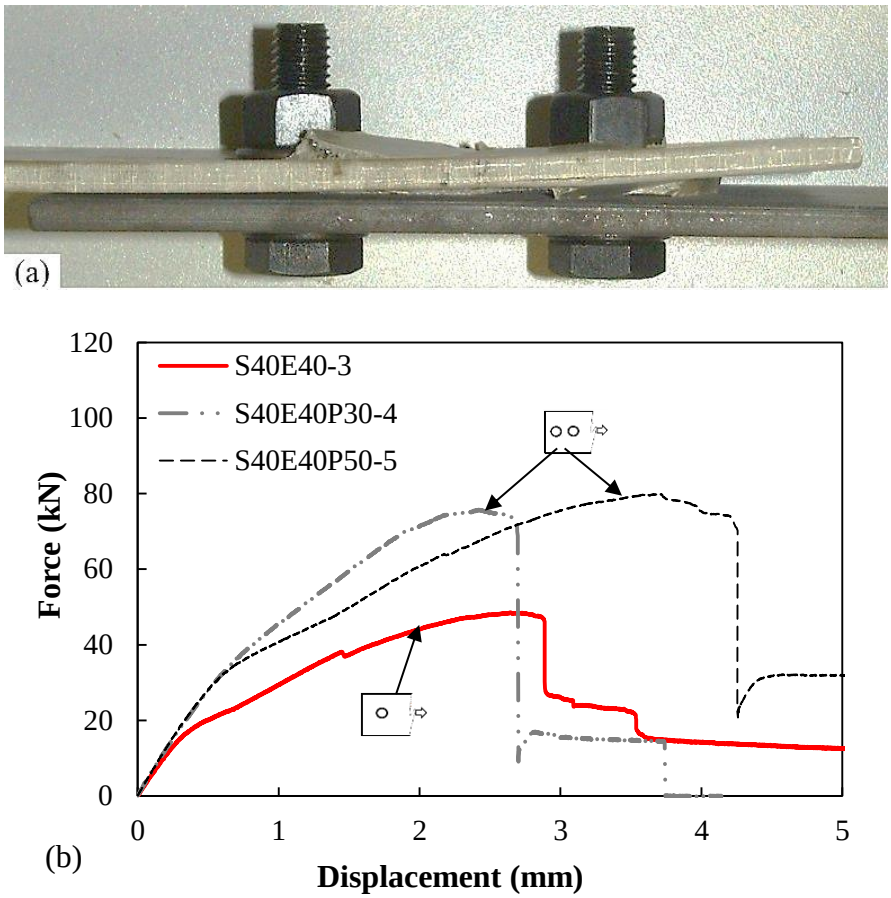


**Figure 6.** (a) Out-of-plane deformation of a two bolt-column, (b) Typical force-displacement curves of S40E40P30 compared to S40E40P50, S40E40

770

771

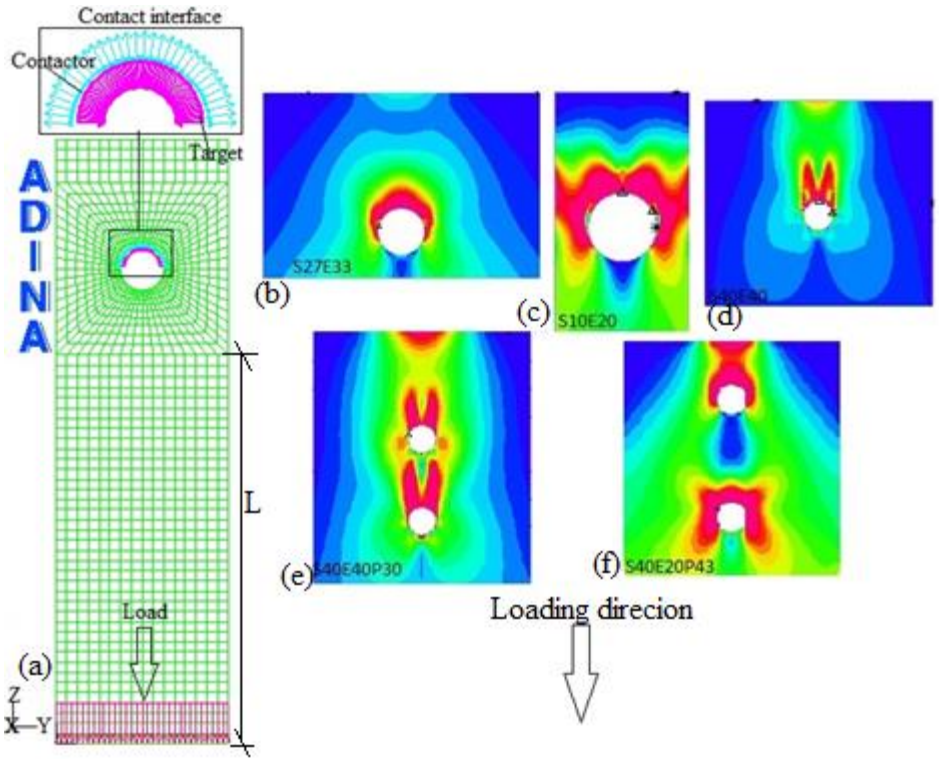


**Figure 7.** (a) Typical 2D model, Post-processing failure modes: (b) bearing, (c) net-section, (d) and (e) shear tear-out, (f) cleavage

772

773

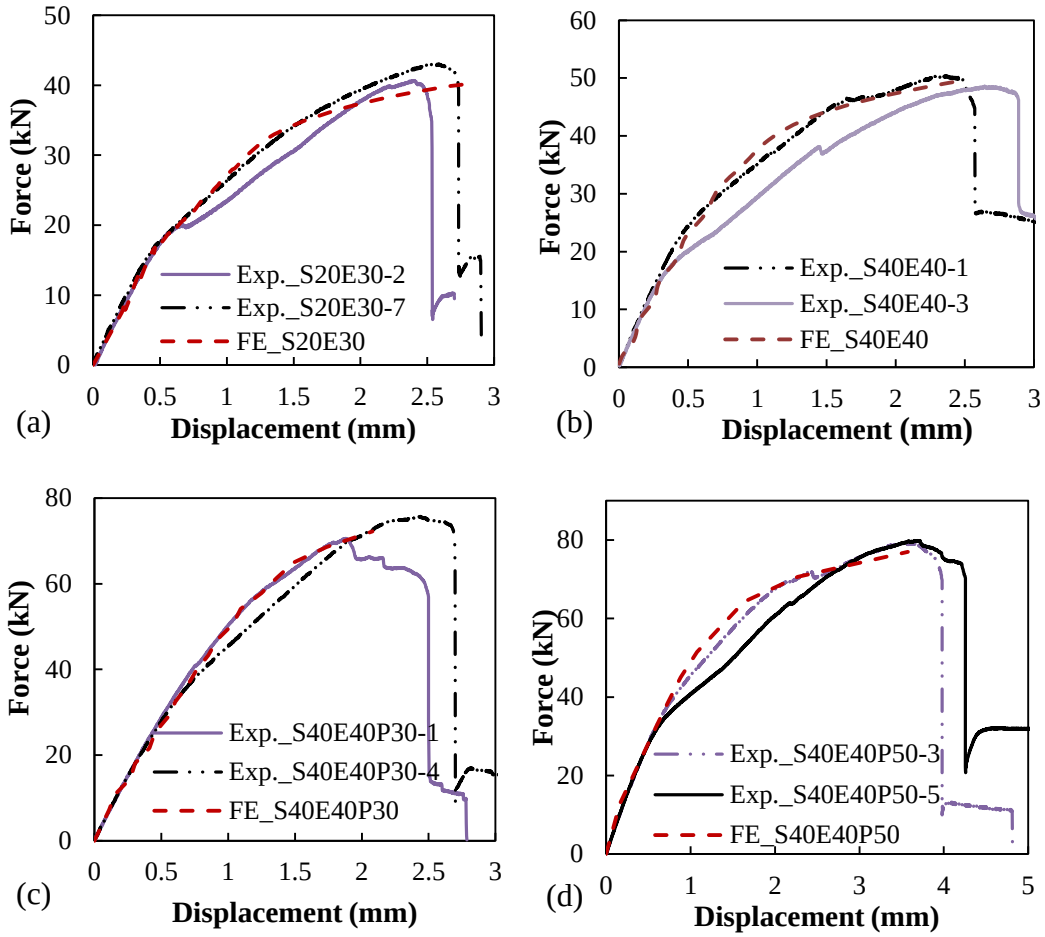


**Figure 8**. Typical force-displacement curves of the experimental compared to finite element models: (a) S20E30, (b) S40E40, (c) S40E40P3, (d) S40E40P50

774

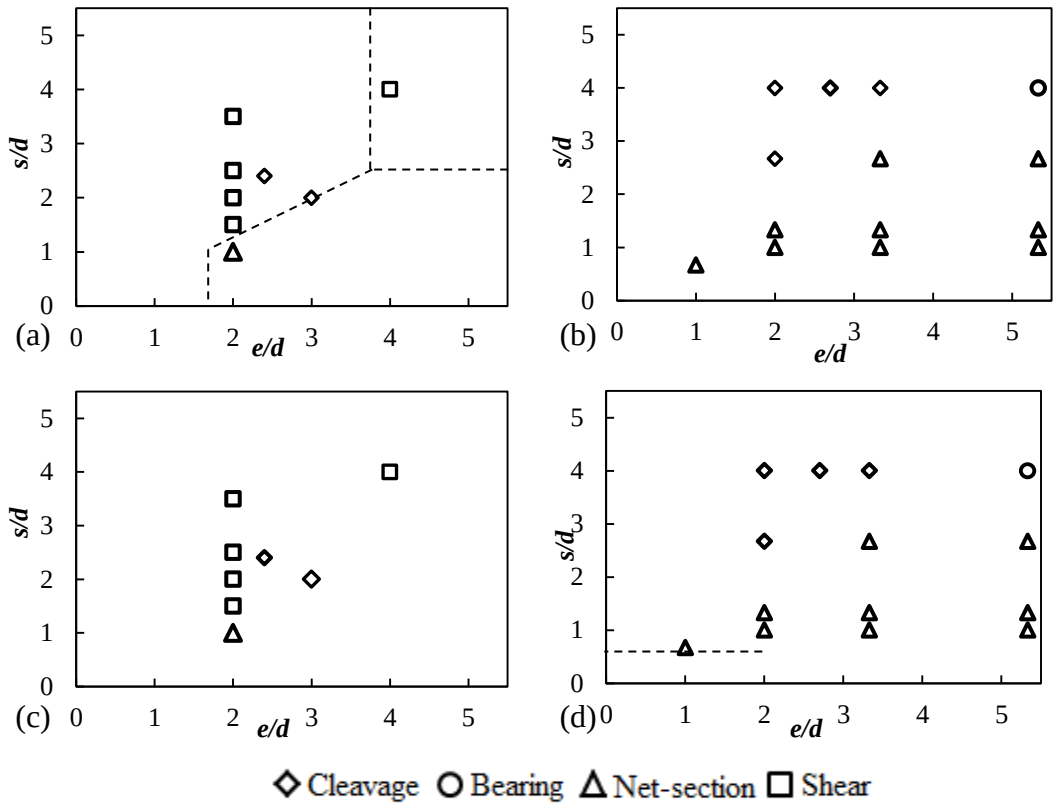


**Figure 9.** Effect of *e/d* and *s/d* on failure modes for one-bolt: (a) FE and Exp. failure modes for highly orthotropic plates; (b) FE and Exp. failure modes for quasi-isotropic plates; (c) [1] and Exp. failure modes for highly orthotropic plates; (d) [1] and Exp. failure modes for quasi-isotropic plates;

775

776

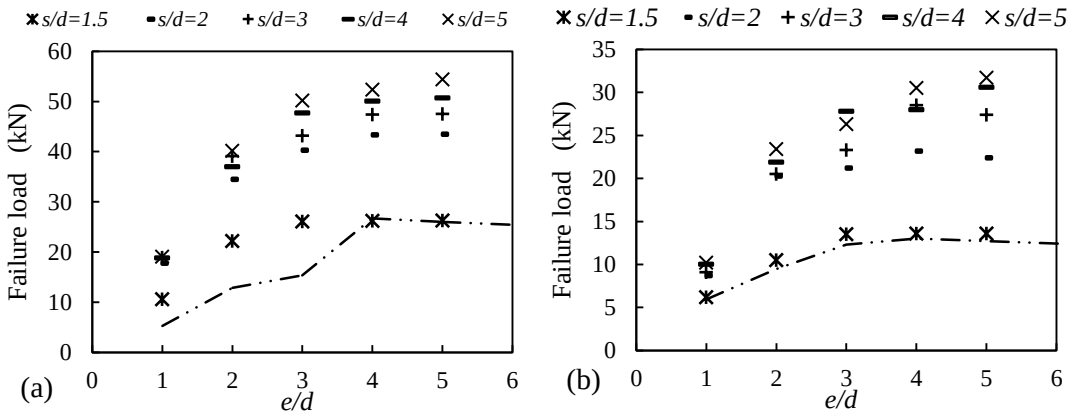


**Figure 10.** Effect of *e/d* and *s/d* on joint strength for one-bolt: (a) FE failure loads for highly orthotropic plates; (b) FE failure loads for quasi-isotropic plates

777

778

779

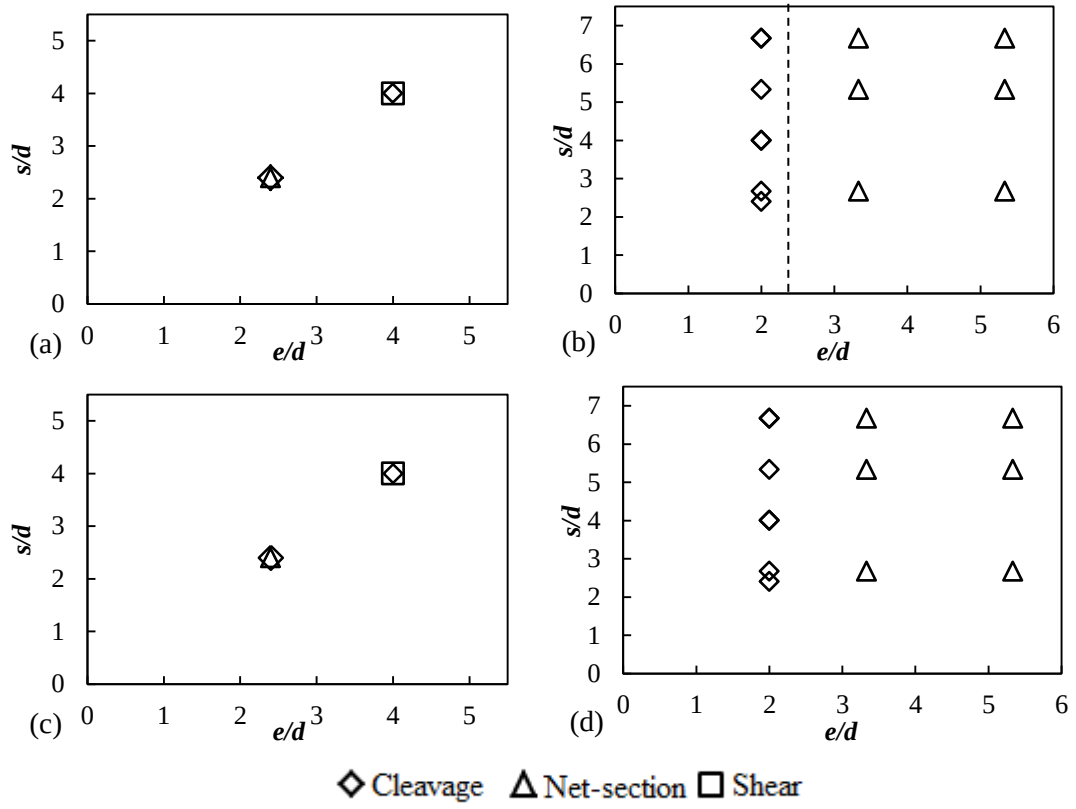


**Figure 11**. Effect of geometric parameters on failure modes for two-bolt: (a) FE and Exp. failure modes for highly orthotropic plates; (b) FE and Exp. failure modes for quasi-isotropic plates; (c) [1] and Exp. failure modes for highly orthotropic plates; (d) [1] and Exp. failure modes for quasi-isotropic plates

780

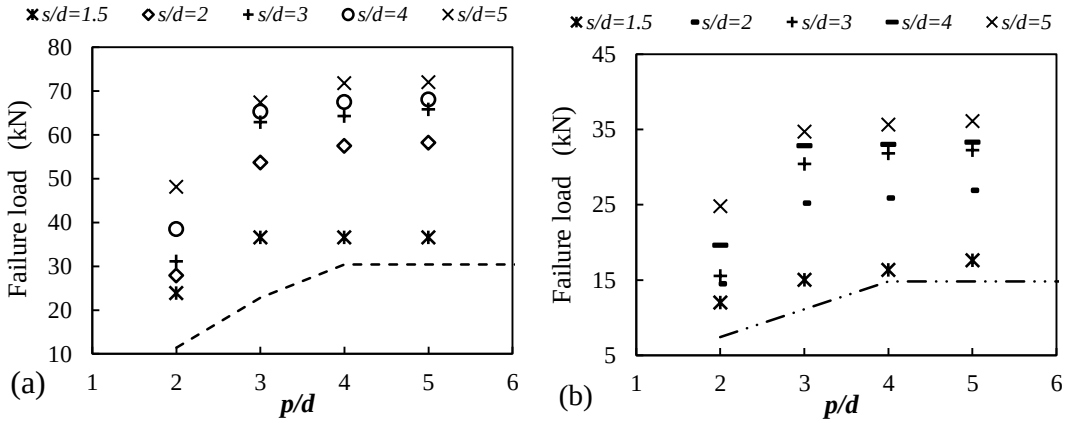


**Figure 12**. Effect of geometric parameters on joint strength for two-bolt: (a) FE failure loads for highly orthotropic plates; (b) FE failure loads for quasi-isotropic plates

781

782

783

784 Table 1. Minimum geometric requirements from design manuals
785 ($d$: diameter of the bolt, $d_h$: bolt-hole)

| | **Pitch (*p*)** | **Gage (*g*)** | **End-distance (*e*)** | **Side-distance (*s*)** |
|---|---|---|---|---|
| ASCE [1] | 4*d* | 4*d* | 4*d for 1bolt*<br>*2d for* multi-row | 1.5*d* |
| EUROCOMP [2] | $4d_h$ | $4d_h$ | $3d_h$; and $s/d_h$ | 0.5*g* |
| CNR -DT [3] | 4*d* | 4*d* | 4*d* | 0.5*g* |
| Strongwell [4] | 5*d* | 5*d* | 3*d* | 2*d* |
| Creative Pultrusion [5] | 3*d* | 3*d* | 3*d* | 2*d* |
| Fibreline Composite [6] | 4*d* | 4*d* | 3.5*d* | 2*d* |

786

787

788

789 Table 2. Mechanical properties of the materials

| Reference | Tested | [10] | [17] |
|---|---|---|---|
| Ratio of $E_{Tt}/E_{Lt}$ | 0.2 | 0.7 | 0.8 |
| Longitudinal modulus $E_{Lt}$ (GPa) | 18.6 | 15.2 | 12.8 |
| Transversal modulus $E_{Tt}$ (GPa) | 4.03 | 10.8 | 10.7 |
| In plane shear modulus $G$ (GPa) | 4.80 | 4.2 | 4.2 |
| Longitudinal tensile strength $f_{uLt}$ (MPa) | 340 | 198 | 166 |
| Transversal tensile strength $f_{uTt}$ (MPa) | 88.4 | 101 | 110 |
| In plane shear strength $f_{ipsh}$ (MPa) | 104.2 | 121 | 117 |
| Longitudinal Poisson ratio $\upsilon_{Lt}$ | 0.33* | 0.28 | 0.28 |

790 ( )* Reported by manufacturer

791

792

Table 3. Tests results of bolted joints

| Tests names | Failure mode | Load (kN) | Displacement at peak load |
|---|---|---|---|
| S20E30-1 | Cleavage | 40.09 | 3.71 |
| S20E30-2 | Cleavage | 44.11 | 2.97 |
| S20E30-3 | Net-section | 39.35 | 3.24 |
| S20E30-4 | Cleavage | 40.86 | 2.46 |
| S20E30-5 | Net-section | 40.68 | 2.39 |
| S20E30-6 | Shear | 40.64 | 2.60 |
| S20E30-7 | Cleavage | 43.03 | 2.59 |
| DS20E30-1 | Cleavage | 43.58 | 2.11 |
| DS20E30-2 | Cleavage | 42.24 | 1.99 |
| DS20E30-3 | Cleavage | 44.39 | 1.87 |
| S40E40-1 | Shear | 50.48 | 2.33 |
| S40E40-2 | Shear | 48.96 | 2.01 |
| S40E40-3 | Shear | 48.56 | 2.65 |
| S40E40-4 | Cleavage | 41.32 | 2.37 |
| S40E40-5 | Shear | 50.05 | 2.28 |
| S40E40P30-1 | Net-section on inner face, shear on outer face | 71.00 | 1.88 |
| S40E40P30-2 | Cleavage | 77.09 | 2.11 |
| S40E40P30-3 | Shear | 77.11 | 2.06 |
| S40E40P30-4 | Shear | 75.53 | 2.42 |
| S40E40P30-5 | Cleavage | 76.65 | 2.06 |
| S40E40P50-1 | Shear | 80.83 | 3.38 |
| S40E40P50-2 | Cleavage | 72.61 | 4.28 |
| S40E40P50-3 | Shear | 80.61 | 3.65 |
| S40E40P50-4 | Shear | 76.58 | 4.28 |
| S40E40P50-5 | Shear | 79.63 | 3.50 |

Table 4. Comparison of experimental to predicted results

| | Ave. $P_{exp}$ (kN) | Exp. FM | Strength (kN) calculated using equations 1 to 7 | | | | | Governed prediction | | $P_{pred}/P_{exp}$ |
|---|---|---|---|---|---|---|---|---|---|---|
| | | | $R_{nt}$ | $R_{sh}$ | $R_{cl}$ | $R_{cl}$ | $R_{br}$ | FL | FM | (2)/(8) |
| (1) | (2) | (3) | (4) | (5) | (6) | (7) | (8) | (9) | (10) | (11) |
| Equation | - | - | 1 or 2 | 3 or 4 | 6 | 7 | 5 | - | - | - |
| S20E30 | **41.3** | **S/C** | 35.5 | 28.8 | 19.5 | 44.3 | 49.4 | **19.5** | **C** | 0.47 |
| DS20E30 | **43.4** | **C** | 35.5 | 28.8 | 19.5 | 44.3 | 49.4 | **19.5** | **C** | 0.45 |
| S40E40 | **47.9** | **S/C** | 50.7 | 40.5 | 38.4* | 48.2* | 49.4 | **40.5** | **S** | 0.85 |
| S40E40P30 | **75.5** | **S/C** | 48.2 | 75.7 | - | - | 74.0 | **48.2** | **N** | 0.64 |
| S40E40P50 | **78.1** | **S** | 64.3 | 99.2 | - | - | 98.7 | **64.3** | **N** | 0.82 |

* Value calculated but not recommended by [1] for $e/d \geq 4$; FL: failure load; FM: failure mode; N: net-section failure; S: shear tear-out failure; C: cleavage failure

Table 5 Model validation

| | Configuration | $P_{exp}$ (kN) | Exp. FM | $P_{FE}$ (kN) | FE FM | $P_{FE}/P_{Exp}$ |
|---|---|---|---|---|---|---|
| Tested/ (1X1) | S30E20 | 41.3 | C/S | 40.2 | C | 0.97 |
| | DS20E30 | 43.4 | C | 40.2 | C | 0.92 |
| | S40E40 | 47.8 | S | 49.7 | S | 1.04 |
| Tested/ (1X2) | S40E40P30 | 75.5 | C/S | 72.2 | S | 0.96 |
| | S40E40P50 | 78.1 | S | 77.0 | S | 0.99 |
| [10]/(1X1) | S07E10 | 6.1 | N | 6.65 | N | 1.09 |
| *d*=19.05mm, | S10E20 | 22 | N | 21.2 | N | 0.96 |
| *t*=9.53 mm | S27E33 | 47.7 | B+N | 46.3 | B | 0.97 |
| [17]/(1X2) | S27E33P43 | 84.2 | N | 82.3 | N | 0.98 |
| *d*=19.05mm, | S40E20P43 | 96.8 | C | 96.15 | C | 0.99 |
| *t*=12.7 mm | S40E33P43 | 102.4 | N | 98.9 | N | 0.96 |
| [17]/(2X1) | S33E20G43 | 96.8 | C | 91.9 | C | 0.95 |
| *d*=19.05mm, | S33E33G43 | 105.8 | N | 101.8 | N | 0.96 |
| *t*=12.7 mm | S47E20G43 | 97.2 | C | 92.1 | C | 0.95 |

Failure modes: N: net-section; C: cleavage; S: shear tear-out

835 Table 6. FE results: failure load (kN)/failure mode

| | | *e/d* | | | | | | | *e/d* | | | | |
|---|---|---|---|---|---|---|---|---|---|---|---|---|---|
| *s/d* | *p/d* | 1 | 2 | 3 | 4 | 5 | *s/d* | *p/d* | 1 | 2 | 3 | 4 | 5 |
| One-bolt (For $E_{Tt}/E_{Lt}$=0.2) | | | | | | | One-bolt (For $E_{Tt}/E_{Lt}$=0.8) | | | | | | |
| 1 | - | 6.2/C | 11.7/N | 12.5/N | 12.5/N | 12.7/N | 1 | - | 4.2/N | 6.3/N | 6.3/N | 6.3/N | 6.3/N |
| 1.5 | - | 10.6/C | 22.2/C | 26.1/N | 26.2/N | 26.3/N | 1.5 | - | 6.2/C | 10.5/C | 13.5/N | 13.6/N | 13.6/N |
| 2 | - | 17.8/C | 34.5/C | 40.2/C | 43.4/N | 43.5/N | 2 | - | 8.7/C | 20.3/C | 21.2/N | 23.2/N | 22.4/N |
| 3 | - | 18.9/C | 35.1/C | 43.2/C | 47.4/S | 47.5/S | 3 | - | 9.1/C | 20.5/C | 23.3/B | 28.5/B | 27.4/B |
| 4 | - | 18.8/C | 37.0/C | 47.7/C | 49.7/S | 50.7/S | 4 | - | 10.0/C | 21.9/C | 27.8/B | 28.0/B | 30.6/B |
| 5 | - | 19.1/C | 40.2/C | 50.2/C | 52.4/S | 54.4/S | 5 | - | 10.2/C | 23.4/C | 26.3/B | 30.5/B | 31.7/B |
| Two-bolt (For $E_{Tt}/E_{Lt}$=0.2) | | | | | | | Two-bolt (For $E_{Tt}/E_{Lt}$=0.8) | | | | | | |
| 1.5 | 2 | 20.3/C | 23.9/S | 25.6/S | 27.9/N | 28.8/N | 1.5 | 2 | 10.1/C | 12.0/N | 12.9/N | 13.1./N | 13.4/N |
| | 3 | 28.2/C | 36.6/N | 37.9/N | 38.2/N | 38.8/N | | 3 | 14.7/C | 15.0/N | 15.1/N | 15.2/N | 15.2/N |
| | 4 | 31.1/C | 36.6/N | 38.0/N | 38.5/N | 38.8/N | | 4 | 14.9/C | 16.3/N | 17.2/N | 17.4/N | 17.4/N |
| | 5 | 32.6/C | 36.6/N | 38.1/N | 38.5/N | 38.9/N | | 5 | 14.9/C | 17.6/N | 17.8/N | 17.6/N | 18.1/N |
| 2 | 2 | 25.4/C | 27.9/S | 31.0/S | 33.9/S | 33.6/S | 2 | 2 | 12.1/C | 14.5/C | 15.5/N | 15.9/N | 16.3/N |
| | 3 | 39.5/C | 53.7/S | 55.8/S | 55.8/S | 55.8/S | | 3 | 21.2/C | 25.2/C | 25.7/N | 25.7/N | 25.8/N |
| | 4 | 40.1/C | 57.5/S | 58.7/S | 65.1/S | 66.3/S | | 4 | 22.1/C | 25.9/C | 26.5/N | 28.0/N | 28.1/N |
| | 5 | 40.7/C | 58.2/S | 59.5/S | 66.9/S | 67.2/S | | 5 | 22.4/C | 26.9/C | 27.2/N | 29.4/N | 29.5/N |
| 3 | 2 | 28.5/C | 31.1/S | 33.6/S | 34.3/S | 34.4/S | 3 | 2 | 14.3/C | 15.5/C | 16.8/N | 17.6/N | 17.6/N |
| | 3 | 54.5/C | 62.9/S | 65.0/S | 69.9/S | 70.4/S | | 3 | 25.4/C | 30.4/C | 31.3/N | 32.3/N | 32.5/N |
| | 4 | 54.8/C | 64.3/S | 67.2/S | 70.3/S | 70.8/S | | 4 | 26.2/C | 31.8/C | 32.1/N | 32.8/N | 33.7/N |
| | 5 | 55.1/S | 65.8/S | 70.3/S | 75.7/S | 76.0/S | | 5 | 27.2/C | 32.2/C | 33.4/N | 35.2/N | 35.4/N |
| 4 | 2 | 36.1/C | 38.5/S | 41.8/S | 43.3/S | 44.8/S | 4 | 2 | 18.9/C | 19.6/C | 19.7/N | 20.9/N | 21.6/N |
| | 3 | 60.2/C | 65.3/S | 69.5/S | 72.2/S | 73.5/S | | 3 | 30.1/C | 32.8/C | 36.4/N | 37.5/N | 37.8/N |
| | 4 | 63.7/C | 67.5/S | 71.4/S | 74.9/S | 76.1/S | | 4 | 30.7/C | 33.0/C | 37.3/N | 38.0/N | 38.1/N |
| | 5 | 63.8/C | 68.1/S | 73.5/S | 77.0/S | 78.6/S | | 5 | 30.7/C | 33.3/C | 38.3/N | 38.4/N | 38.4/N |
| 5 | 2 | 44.7/C | 48.1/S | 51.1/S | 53.3/S | 54.6/S | 5 | 2 | 22.3/C | 24.8/C | 25.8/N | 26.3/N | 26.9/N |
| | 3 | 63.4/C | 67.4/S | 69.8/S | 75.6/S | 75.6/S | | 3 | 31.1/C | 34.7/C | 39.2/N | 40.8/N | 41.8/N |
| | 4 | 63.5/C | 71.8/S | 75.3/S | 78.1/S | 79.0/S | | 4 | 31.6/C | 35.6/C | 39.2/N | 41.1/N | 42.0/N |
| | 5 | 64.2/C | 72.0/S | 78.8/S | 79.9/S | 80.3/S | | 5 | 32.0/C | 36.1/C | 39.4/N | 41.5/N | 42.0/N |

836 N: net-section failure; C: cleavage failure; S: shear tear-out failure; B: bearing failure

837

838

839

840 Table 7. Experimental failure modes

| One bolt (1X1) | | | | | | Two-bolt (1X2) | | | |
|---|---|---|---|---|---|---|---|---|---|
| *e/d* | *s/d* | FM | *e/d* | *s/d* | FM | *p/d* | *e/d* | *s/d* | FM |
| $E_{Tt}/E_{Lt}$=0.2 Tested | | | $E_{Tt}/E_{Lt}$ =0.7 [13] | | | $E_{Tt}/E_{Lt}$=0.2 Tested | | | |
| 3 | 2 | C | 1 | 0.7 | N | 3 | 4 | 4 | S/C |
| 4 | 4 | S | 10.7 | 0.7 | N | 5 | 4 | 4 | S |
| $E_{Tt}/E_{Lt}$=0.3 [17] | | | 2 | 1 | N | $E_{Tt}/E_{Lt}$ =0.3[36] | | | |
| 2 | 1 | N | 3.3 | 1 | N | 4 | 2.4 | 2.4 | N/C |
| 2 | 1.5 | S | 5.3 | 1 | N | $E_{Tt}/E_{Lt}$ =0.8 [37] | | | |
| 2 | 2 | S | 2 | 1.3 | N | 4.3 | 2 | 2.7 | C |
| 2 | 2.5 | S | 3.3 | 1.3 | N | 4.3 | 3.3 | 2.7 | N |
| 2 | 3.5 | S | 5.3 | 1.3 | N | 4.3 | 5.3 | 2.7 | N |
| $E_{Tt}/E_{Lt}$=0.3[36] | | | 2 | 2.7 | C | 4.3 | 2 | 4 | C |
| 2.4 | 2.4 | C | 3.3 | 2.7 | N | 4.3 | 3.3 | 4 | N |
| | | | 5.3 | 2.7 | N | 4.3 | 5.3 | 4 | N |
| | | | 10.7 | 2.7 | N | 4.3 | 2 | 5.3 | C |
| | | | 2 | 4 | C | 4.3 | 3.3 | 5.3 | N |
| | | | 3.3 | 4 | C | 4.3 | 5.3 | 5.3 | N |
| | | | 5.3 | 4 | B | 4.3 | 2 | 6.7 | C |
| | | | 1 | 6.7 | C | 4.3 | 3.3 | 6.7 | N |
| | | | 2 | 6.7 | C | 4.3 | 5.3 | 6.7 | N |
| | | | 3.3 | 6.7 | C | | | | |
| | | | 5.3 | 6.7 | B | | | | |
| | | | 10.7 | 6.7 | B | | | | |
| | | | $E_{Tt}/E_{Lt}$=0.8 [14] | | | | | | |
| | | | 2.7 | 4 | C | | | | |

841
842